

## THE REMARKABLE MID-INFRARED JET OF THE MASSIVE YOUNG STELLAR OBJECT G35.20–0.74

JAMES M. DE BUIZER

Gemini Observatory, Casilla 603, La Serena, Chile; jdebuizer@gemini.edu  
Received 2006 February 23; accepted 2006 March 15; published 2006 April 6

### ABSTRACT

The young massive stellar object G35.20–0.74 was observed in the mid-infrared using T-ReCS on Gemini South. Previous observations have shown that the near-infrared emission has a fanlike morphology that is consistent with emission from the northern lobe of a bipolar radio jet known to be associated with this source. Mid-infrared observations presented in this Letter show a monopolar jet-like morphology as well, and it is argued that the mid-infrared emission observed is dominated by thermal continuum emission from dust. The mid-infrared emission nearest the central stellar source is believed to be directly heated dust on the walls of the outflow cavity. The hydroxyl, water, and methanol masers associated with G35.20–0.74 are spatially located along these mid-infrared cavity walls. Narrow jet or outflow cavities such as this may also be the locations of the linear distribution of methanol masers that are found in association with massive young stellar objects. The fact that G35.20–0.74 has mid-infrared emission that is dominated by the outflow, rather than disk emission, is a caution to those who consider mid-infrared emission from young stellar objects to come only from circumstellar disks.

*Subject headings:* circumstellar matter — infrared: ISM — ISM: individual (G35.20-0.74) — ISM: jets and outflows — masers — stars: formation

### 1. INTRODUCTION

While molecular outflows are an apparently ubiquitous phenomenon in regions of high-mass star formation (Shepherd & Churchwell 1996; Zhang et al. 2001; Beuther et al. 2002), clear examples of individual young massive stars with well-defined bipolar jets are relatively few. One such example is G35.20–0.74, a massive star formation region containing an early B-type star surrounded by an ultracompact H II region with a bipolar jet-like radio structure. Water, OH, and methanol masers (Forster & Caswell 1989; Hutawarakorn & Cohen 1999) are all associated with this massive young stellar object (YSO), though the nature of their relationship with respect to G35.20–0.74 is still unclear.

This jet and outflow have recently been observed in the near-infrared (NIR) by Fuller et al. (2001) and in the mid-infrared (MIR) at low spatial resolution ( $\sim 1''$ ) by De Buizer et al. (2005). The nature and structure of the thermal infrared emission seen from this outflow in these two studies has prompted this high spatial resolution ( $\sim 0.35''$  at  $11.7 \mu\text{m}$ ) MIR follow-up study. In this Letter, I explore the characteristics of the MIR emission in G35.20–0.74 and relationships between the detailed morphologies of the infrared emission, masers, and radio continuum emission.

### 2. OBSERVATIONS

Observations of G35.20–0.74 were carried out at Gemini South on the night of 2005 July 12 through patchy clouds. Imaging was performed with the Thermal-Region Camera and Spectrograph (T-ReCS) using the Si-5 filter ( $\lambda_c = 11.7 \mu\text{m}$ ,  $\Delta\lambda = 1.1 \mu\text{m}$ ) and Qa filter ( $\lambda_c = 18.3 \mu\text{m}$ ,  $\Delta\lambda = 1.6 \mu\text{m}$ ). T-ReCS utilizes a Raytheon  $320 \times 240$  pixel Si:As impurity-band conduction array that is optimized for use in the 7–26  $\mu\text{m}$  wavelength range. The pixel scale is  $0''.089 \text{ pixel}^{-1}$ , yielding a field of view of  $28''.8 \times 21''.6$ . Co-added frames were saved every 10 s, and the telescope was nodded every 30 s. The co-added frames were examined individually during the data reduction process, and those plagued by clouds (i.e., show-

ing high or variable background or decreased source flux) were discarded. In both filters the northern and southern radio jet regions were imaged, yielding final mosaicked images with effective field of views of approximately  $28'' \times 35''$ . The  $8''$  overlapping region was used to register the northern and southern images of each mosaic. However, the individual images were cropped before they were mosaicked, so the final mosaic has the same signal-to-noise ratio across the whole image. The final *effective* exposure times for the mosaics presented here are therefore 140 s at  $11.7 \mu\text{m}$  and 180 s at  $18.3 \mu\text{m}$ .

Flux calibration was achieved by observing the MIR standard star HD 169916 ( $\lambda$  Sgr) at similar air masses to the G35.20–0.74 observations. The assumed flux densities for HD 169916 were taken to be  $22.29 \text{ Jy}$  at  $11.7 \mu\text{m}$  and  $9.24 \text{ Jy}$  at  $18.3 \mu\text{m}$ . These assumed standard-star flux densities were found by convolving the spectral irradiance templates of the stars from Cohen et al. (1999) with the given T-ReCS filter transmission profile. Derived flux densities for the entire region of G35.20–0.74 are measured to be  $3.06 \pm 0.09 \text{ Jy}$  at  $11.7 \mu\text{m}$  and  $46.87 \pm 3.66 \text{ Jy}$  at  $18.3 \mu\text{m}$  using a square aperture of  $6''.9 \times 13''.5$ . These flux densities are quoted with their  $1 \sigma$  total error, which is a quadrature addition of the statistical variation from the aperture photometry (due to the standard deviation of the background array noise) and the flux calibration error. The flux calibration error was found from the standard deviation of the variation of the standard-star flux density in each co-added nod position. Since the science and standard-star images were cleaned of any effects from clouds, the quoted errors are thought to be robust; however, the errors were calculated using all available data. Comparisons with the lower angular resolution observations in De Buizer et al. (2005) show the values derived here to be consistent with those derived in that previous work.

### 3. DISCUSSION

The mosaicked images at  $11.7$  and  $18.3 \mu\text{m}$  are presented in Figure 1. These images are cropped to show only the parts of the field that have MIR sources. No significant MIR emission was detected outside these cropped areas at a  $3 \sigma$  upper

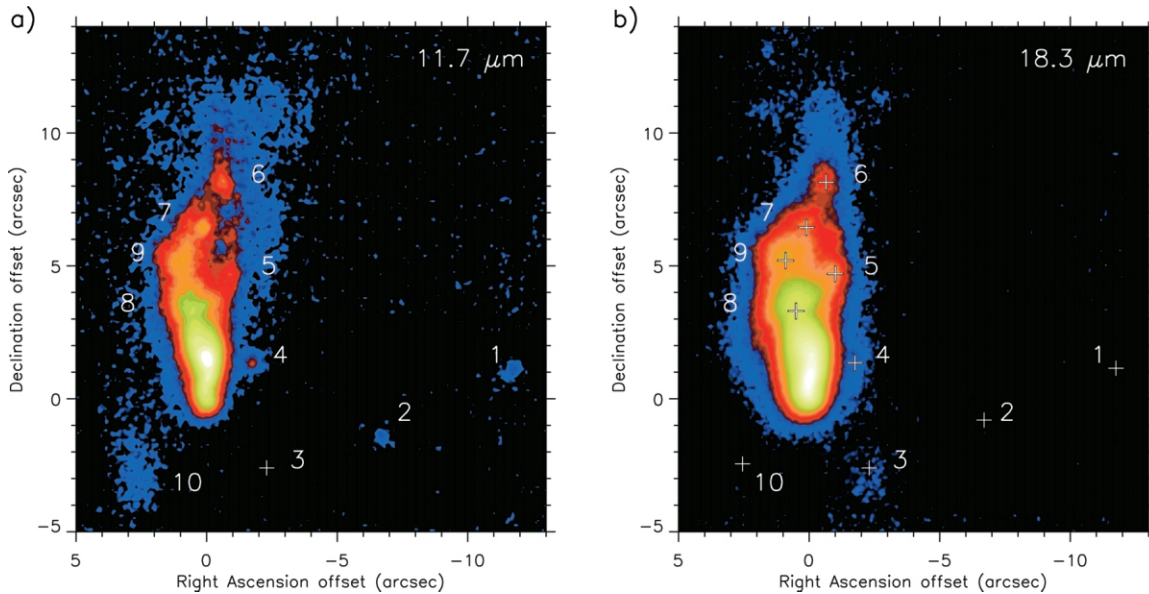


FIG. 1.—The region of G35.20–0.74 in false color as seen at (a) 11.7  $\mu\text{m}$  and (b) 18.3  $\mu\text{m}$  with T-ReCS. Plus signs in (b) show the locations of individual MIR sources at 11.7  $\mu\text{m}$  and are numbered by increasing right ascension. The plus sign in (a) shows the 18.3  $\mu\text{m}$  location of source 3, which is not seen at 11.7  $\mu\text{m}$ . The origin is the location of the radio continuum source G35.2N, R.A. = 18<sup>h</sup>58<sup>m</sup>13<sup>s</sup>033, decl. = +01<sup>o</sup>40′36″14 (J2000) (A. G. Gibb 2006, private communication).

limit of 41 mJy arcsec<sup>-2</sup> at 11.7  $\mu\text{m}$  and 283 mJy arcsec<sup>-2</sup> at 18.3  $\mu\text{m}$ . Sources 1, 2, and 10 are seen at 11.7  $\mu\text{m}$  but not at 18.3  $\mu\text{m}$ , and source 3 is seen at 18.3  $\mu\text{m}$  but not 11.7  $\mu\text{m}$ . Source 4 is marginally detected at 18.3  $\mu\text{m}$ . The remaining sources are detected at both wavelengths and are mostly knots of emission associated with the MIR monopolar jet of G35.20–0.74. The origin of Figure 1 is the expected location of the outflow source itself. This source is a B2.6 star (as derived from the 8.5 GHz flux density of Gibb et al. [2003] and using the method described in De Buizer et al. [2005]) that can be seen as an ultracompact H II region in the radio and has been dubbed G35.2N.

### 3.1. Relations to Radio Continuum and NIR Emission

The MIR images were registered with respect to the NIR *K* and *L'* images of Fuller et al. (2001). Very accurate relative astrometry (<0″15) was achieved because of the presence of three compact MIR sources (1, 2, and 4) that are also present in the *K* and/or *L'* images. The absolute astrometry of the NIR images (and, consequently, the MIR images) comes from matching up NIR point sources with their optical counterparts found in the USNO-B1.0 astrometric catalog. The estimates of the 1  $\sigma$  absolute uncertainty in these coordinates are 0″3 for right ascension and 0″1 for declination.

Figure 2a shows the *K* emission (white contours) overlaid on the 11.7  $\mu\text{m}$  image, and Figure 2b shows the *L'* emission (gray contours) overlaid on the 18.3  $\mu\text{m}$  image. The *L'* emission from the jet looks very similar to what is seen in the MIR. The *K* emission appears to be dominated more by the material in the north, farther along the outflow axis, with very little emission down near the outflow source itself. The convex structure seen in the NIR breaks up into separate MIR components (knots 5 and 8) and therefore is probably not a bow shock as implied by Fuller et al. (2001).

The *L'* images of Fuller et al. (2001) show what they claim is weak NIR emission from the southern jet of G35.20–0.74

(see Fig. 2b). Interestingly, this emission is extremely weak at *K*, bright at *L'*, and not detected at 11.7  $\mu\text{m}$ , but it is present at 18.3  $\mu\text{m}$  (source 3 in Fig. 1).

The MIR images were also registered with respect to the high-resolution 8.5 GHz radio continuum images of Gibb et al. (2003) (Fig. 2a, gray contours) and with the low-resolution 15 GHz radio continuum image of Heaton & Little (1988) (Fig. 2b, white contours). The 1  $\sigma$  relative astrometric error between the MIR and radio continuum images is estimated to be 0″34 in right ascension and 0″18 in declination. The MIR and NIR images and contours shown in Figure 2 have been shifted +0″023 (+0″35) in right ascension to place G35.2N on the infrared outflow axis (this is approximately the estimated 1  $\sigma$  astrometric uncertainty).

In Figure 2b, it can be seen that the overall extent of the northern radio lobe is comparable to that of the MIR emission. There is also considerable MIR emission coming from the central radio continuum–emitting region near the outflow source; however, there is no MIR emission from the southern radio peaks. G35.2N is also the location of one of the two millimeter peaks (Gibb et al. 2003) in this region (Fig. 2b, plus signs).

The two northernmost radio knots lie close to, but are not exactly coincident with, MIR sources 6 and 7. For these knots, the radio and the MIR may be tracing slightly different emitting regions within the knots themselves.

### 3.2. Nature of the Mid-Infrared Emission

MIR emission from outflows has been detected previously (e.g., Noriega-Crespo 2004); however, these outflows have been claimed to be dominated by shock lines of H<sub>2</sub> contained within the filters used. For the observations presented here, there are no H<sub>2</sub> lines within the bandpass of either the 11.3 or the 18.3  $\mu\text{m}$  filter. There is a possibility that there may be some contribution to the emission at 11.7  $\mu\text{m}$  because of PAH emission; however, this is not a concern at 18.3  $\mu\text{m}$ . The steeply rising spectral slope from *L'* to 18.3  $\mu\text{m}$  of the narrow, elongated

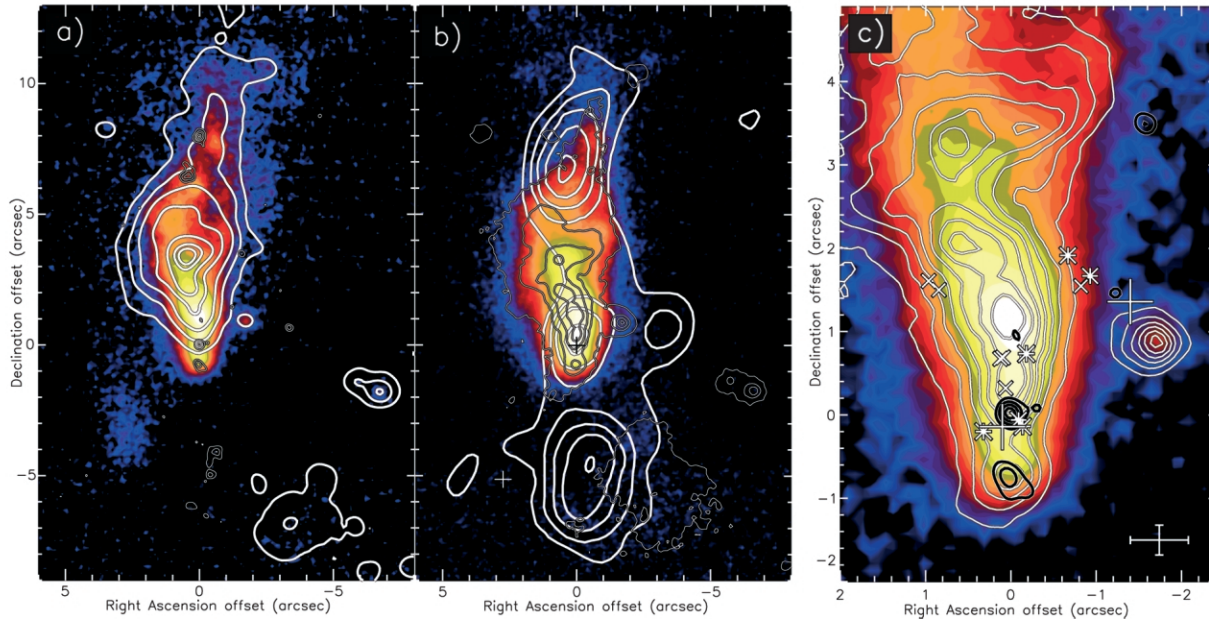


FIG. 2.—The G35.20–0.74 jet as seen at different wavelengths. (a) The  $11.7\ \mu\text{m}$  image in false color overlaid with  $K$ -band emission from Fuller et al. (2001, *white contours*) and the  $8.5\ \text{GHz}$  high-resolution radio continuum emission of Gibb et al. (2003, *gray contours*). (b) The  $18.3\ \mu\text{m}$  image in false color overlaid with the low-resolution  $15\ \text{GHz}$  radio continuum image of Heaton & Little (1988, *white contours*) and  $L'$  image from Fuller et al. (2001, *gray contours*). (c) Zoom in on the central region of the  $11.7\ \mu\text{m}$  image in false color, the  $L'$  contours in white and the high-resolution radio continuum contours in black. The OH masers of Hutawarakorn & Cohen (1999) are shown as asterisks, water masers of Forster & Caswell (1989) as crosses, and methanol masers of A. G. Gibb (2006, private communication) as large plus signs. The bars at lower right show the  $\pm 1\ \sigma$  relative astrometric uncertainty between the radio continuum and NIR.

infrared emission coincident with and immediately north of the position of G35.2N demonstrates that the infrared emission here is dominated by longer wavelength continuum emission. Therefore, the nature of the infrared emission is concluded to be predominantly continuum dust emission from the outflow cavity walls. This cavity was created by the molecular outflow, which punched a hole in the dense molecular material surrounding the young stellar source at the center of G35.20–0.74. The central source is mostly likely directly heating the walls of this cavity. The northern lobe of the outflow was found to be slightly blueshifted toward Earth (i.e., in CO by Gibb et al. 2003; in C I by Little et al. 1998). Given this fortuitous geometry, we can see directly into the outflow cavity as a consequence of the clearing away of material along our line of sight by the outflow itself.

The sources farther north of G35.20–0.74, namely, sources 5–9, are expected to be knots of dust either in the outflow itself or clumps of preexisting material that are being impinged upon by the outflow. Source 6 lies  $19,200\ \text{AU}$  from G35.2N and is still at an estimated dust color temperature of  $112\ \text{K}$ . This is based on the  $11.7$  and  $18.3\ \mu\text{m}$  flux densities of this source and neglects the possible effects of silicate absorption (see De Buizer et al. [2005] for method and limitations). What is heating the dust this far out? Smaller dust grains can be heated out to farther distances than large dust grains. The typical size range of interstellar grains is believed to be  $0.003$ – $10\ \mu\text{m}$ , and typical grain compositions include smooth astronomical silicates, graphite, and silicon carbide (Laor & Draine 1993; Draine & Lee 1984). In the following I use the equation for dust temperature given by Sellgren et al. (1983) and the ultraviolet and infrared emissivities of Draine & Lee (1984). Assuming the dust is made up of smooth astronomical silicates, dust with a lower size limit of  $0.003\ \mu\text{m}$  can be heated to  $112\ \text{K}$  only out

to  $\sim 16,000\ \text{AU}$  by a B2.6 star. If the dust is made of graphite, one could heat out to the distance of source 6 with grains having a typical size of  $0.005\ \mu\text{m}$ , still near the lower size limit. However, if silicon carbide is the assumed composition of the dust, then one can get heating out much farther than source 6, namely,  $\sim 52,000\ \text{AU}$  at the  $0.003\ \mu\text{m}$  lower size limit. There is a possibility of some contribution from shock heating, although Fuller et al. (2001) claim no detection of shock-excited  $\text{H}_2$  in the region. Beaming of the MIR emission along the outflow axis, rather than the isotropic emission assumed in the above calculations, could also help in heating grains farther out. Interestingly, the MIR luminosity derived from the dust color temperature gives an estimated value of  $1.6 \times 10^3 L_\odot$ . Assuming the MIR luminosity is all the luminosity of the source (an obvious underestimate) and calculating a spectral type from that bolometric luminosity using the method from De Buizer et al. (2005) gives a value of  $\sim \text{B3}$ , consistent with the radio-derived spectral type. In summary, all of the dust, even as far out as source 6, *can* indeed be heated directly by G35.2N, depending on dust composition and size (as well as beaming), though we cannot rule out contributions from other possible heating mechanisms.

As discussed in § 3.1, MIR source 3, coincident with NIR emission from the presumed infrared southern counterjet, does not have a smoothly increasing spectral slope typical of dust continuum emission but instead is only present at  $L'$  and  $18.3\ \mu\text{m}$ . This implies that the emission in this southern source is dominated by line emission of some kind. The usual suspects are (1)  $\text{H}_2$  emission from shocks, although Fuller et al. (2001) claim no detection of  $\text{H}_2$  in the region; (2) PAH emission from the photodissociation region of the outflow interface with the molecular cloud, although the  $L'$  and  $18.3\ \mu\text{m}$  filters do not encompass any PAH features; and (3)  $[\text{Fe II}]$  emission from

shocks. This last one may be a possibility, since [Fe II] lines are found in both filter bandpasses, but spectroscopy will be needed in order to know for sure.

### 3.3. Masers

The positions of the OH masers from Hutawarakorn & Cohen (1999) and water masers from Forster & Caswell (1989) are shown in Figure 2c (*asterisks and crosses, respectively*). The positions of these maser sources with respect to the radio continuum emission were taken from Gibb et al. (2003). There are also methanol masers plotted in Figure 2c (*large plus signs*), which were found by A. G. Gibb (2006, private communication) and have positions known to 0.2 with respect to the radio continuum.

Interestingly, the combined distribution of the masers is in a V shape, with its apex near the G35.2N source itself. From their positions with respect to the NIR and MIR emission, the masers appear to be tracing the outflow cavity walls. In the case of the OH and water masers, they may be excited to emit here by the slower oblique shocks created by the outflow on the cavity walls. Methanol masers, on the other hand, are believed to be excited by MIR radiation (e.g., Sobolev & Deguchi 1994; Sobolev et al. 1997). The copious amount of MIR emission associated with this outflow source implies that at least the pumping mechanism needed for the generation of methanol masers exists on such outflow cavity walls.

Given the narrow opening angle of this outflow cavity as seen in the MIR and the fact that methanol masers are often found in linear distributions (see, e.g., Norris et al. 1993), it is possible that methanol masers in general are associated with the cavity walls of outflowing young massive stars. Previous observations reported in De Buizer (2003) found the majority of linear methanol maser distributions in that sample to lie at position angles similar to H<sub>2</sub> emission expected to trace outflows from the host YSOs. Furthermore, other sources such as NGC 7538 IRS 1 (De Buizer & Minier 2005) have been observed in the MIR to have outflow-like MIR emission at the same position angle as other outflow indicators (CO in the case of NGC 7538 IRS 1), as well as having a linear methanol maser distribution at a similar position angle. All of this may point to a scenario in which the linearly distributed methanol masers may be associated more generally with outflows of massive

YSOs, and not with circumstellar disks as was previously thought (e.g., Norris et al. 1993).

### 3.4. Implications for Mid-Infrared-bright YSOs

There is a tendency to think that if MIR emission is detected in a young stellar object (especially if it appears elongated in its morphology) that it is emission from a circumstellar disk (e.g., Lada & Lada 2003). Recent observations and theories (e.g., Miroshnichenko et al. 1999) have shown that, at least for the more massive YSOs, the dominant source of MIR emission comes from an accretion envelope. These accretion envelopes may be elongated as well (De Buizer et al. 2005). The observations presented here show that one must take into account another source of MIR continuum emission. On a 3–4 m telescope (De Buizer et al. 2005), or with the resolution of the *Spitzer Space Telescope*, the MIR emission from G35.20–0.74 could be misinterpreted as a circumstellar disk. Only recently, with the increase of MIR instruments on 8–10 m telescopes, have we begun to resolve sources such as G35.20–0.74 with such detail as to discern their true MIR emission as being outflow related (e.g., NGC 7538 IRS 1; De Buizer & Minier 2005).

Therefore, one should be cautious when trying to infer disk properties from unresolved or partially resolved sources, since the outflow cavities of YSOs can be the dominant source of MIR continuum emission. On the other hand, the mere presence of such outflow cavities with small opening angles implies the presence of collimating accretion disks at the bases of the outflows. So, while MIR emission may not always be a *direct* tracer of circumstellar disks and their properties, the presence of such emission in the near circumstellar environment of a YSO may still indirectly indicate the presence of a disk.

This work is based on observations obtained at the Gemini Observatory, which is operated by the Association of Universities for Research in Astronomy, Inc., under a cooperative agreement with the NSF on behalf of the Gemini partnership: the NSF (US), the PPARC (UK), the NRCC (Canada), CONICYT (Chile), the ARC (Australia), CNPq (Brazil), and CONICET (Argentina). I would like to thank James Radomski for his illuminating discussions, which helped in the writing of this Letter.

### REFERENCES

- Beuther, H., Schilke, P., Sridharan, T. K., Menten, K. M., Walmsley, C. M., & Wyrowski, F. 2002, *A&A*, 383, 892  
 Cohen, M., Walker, R. G., Carter, B., Hammersley, P., Kidger, M., & Noguchi, K. 1999, *AJ*, 117, 1864  
 De Buizer, J. M. 2003, *MNRAS*, 341, 277  
 De Buizer, J. M., & Minier, V. 2005, *ApJ*, 628, L151  
 De Buizer, J. M., Radomski, J. T., Telesco, C. M., & Piña, R. K. 2005, *ApJS*, 156, 179  
 Draine, B. T., & Lee, H. M. 1984, *ApJ*, 285, 89  
 Forster, J. R., & Caswell, J. L. 1989, *A&A*, 213, 339  
 Fuller, G. A., Zijlstra, A. A., & Williams, S. J. 2001, *ApJ*, 555, L125  
 Gibb, A. G., Hoare, M. G., Little, L. T., & Wright, M. C. H. 2003, *MNRAS*, 339, 1011  
 Heaton, B. D., & Little, L. T. 1988, *A&A*, 195, 193  
 Hutawarakorn, B., & Cohen, R. J. 1999, *MNRAS*, 303, 845  
 Lada, C. J., & Lada, E. A. 2003, *ARA&A*, 41, 57  
 Laor, A., & Draine, B. T. 1993, *ApJ*, 402, 441  
 Little, L. T., Kelly, M. L., & Murphy, B. T. 1998, *MNRAS*, 294, 105  
 Miroshnichenko, A., Ivezić, Ž., Vinković, D., & Elitzur, M. 1999, *ApJ*, 520, L115  
 Noriega-Crespo, A., et al. 2004, *ApJS*, 154, 352  
 Norris, R. P., Whiteoak, J. B., Caswell, J. L., Wieringa, M. H., & Gough, R. G. 1993, *ApJ*, 412, 222  
 Sellgren, K., Werner, M. W., & Dinerstein, H. L. 1983, *ApJ*, 271, L13  
 Shepherd, D. S., & Churchwell, E. 1996, *ApJ*, 457, 267  
 Sobolev, A. M., Cragg, D. M., & Godfrey, P. D. 1997, *A&A*, 324, 211  
 Sobolev, A. M., & Deguchi, S. 1994, *A&A*, 291, 569  
 Zhang, Q., Hunter, T. R., Brand, J., Sridharan, T. K., Molinari, S., Kramer, M. A., & Cesaroni, R. 2001, *ApJ*, 552, L167